DRAFT

Proceedings of ASME Turbo Expo 2017: Gas Turbine Technical Conference and Exposition GT2017
July 26-30, 2017, Charlotte, NC, USA

GT2017-64743

A ONE-DIMENSIONAL GAS DYNAMICS CODE FOR TURBOCHARGER TURBINE PULSATING FLOW PERFORMANCE MODELLING

Adam Feneley
Institute of Energy Futures,
Brunel University London
London, United Kingdom

Apostolos Pesiridis
Institute of Energy Futures,
Brunel University London
London, United Kingdom

Hua Chen
National Laboratory of Engine
Turbocharging Technologies
China

ABSTRACT

As governments around the world ramp up their efforts to reduce CO_2 emissions, downsizing internal combustion engines has become a dominant trend in the automotive industry. Air charging systems are being utilised to increase power density and therefore lower emissions by downsizing internal combustion engines. Turbocharging represents the majority of these air charging systems, which are commonly adopted for commercial and passenger vehicles. The process of matching turbomachinery to an engine during early-stage development is important to achieving maximum engine performance in terms of power output and the reduction of emissions.

Despite on-engine conditions providing highly unsteady gas flows, current turbocharger development commonly uses performance maps that are produced from steady state measurements. There are other significant sources of error to be found in early stage turbocharger performance prediction, such as the omission of heat transfer effects, and the use of data extrapolation methods to cover the entire operating range of a device from limited data sets. Realistic engine conditions provide a complex heat transfer scenario, which is dependent upon load history and the component layout of the engine bay. Heat transfer effects are particularly prevalent at low engine loads, whilst pulsating effects are significant at both high and low engine speeds (and therefore exhaust pulse frequency). Compressor maps are often provided by manufacturers with a level of heat transfer corresponding to a gas stand test, not realistic engine conditions. This causes a mismatch when using the aforementioned maps in commercial engine codes. This reduces the quality of overall engine performance predictions, since as the temperature of the exhaust gas on the turbine side rises, the performance prediction increasingly deviates from the usual adiabatic assumption used in simulations.

In the present work, a one-dimensional unsteady flow model has been developed to predict the performance of a vaneless turbine under pulsating inlet conditions, with scope to account for heat transfer effects. Flow within the volute is considered to be one-dimensional and unsteady, with mass addition and withdrawal used to simulate the gas flow between the volute and rotor. Rotor passages are also treated as one-dimensional and unsteady, with the equations being solved by the method of characteristics. This model is able to simulate the circumferential feeding of the rotor from the casing, unlike many previous zero and one-dimensional models. Building upon previous work, the basis of this code has been constructed in C++ with future integration with other modern gas dynamics codes in mind. By providing the appropriate instantaneous operating conditions at specified time intervals, a code such as this could theoretically negate the need for maps produced by steady-state data.

INTRODUCTION

As a response to increasingly strict emissions regulations around the world, engine manufacturers are actively downsizing their engines in order to increase power density and reduce emissions. Turbocharging is a key enabler when downsizing engines, and the market for turbochargers is forecast to grow with a compound annual growth rate of 10.21% for 5 years from 2015, leading to a market worth an estimated $22.1bn in 2020 (up from $13.6bn). [1]

During the early stages of the engine design process, engine cycle simulation, including the simulation of turbocharger performance, is commonly used in industry. Typically, many different engine-turbocharger variations are assessed at a range of steady-state design points; usually these design points correspond to a standard drive cycle.

However, realistically turbochargers do not operate in steady state conditions on internal combustion engines, with the exception of some high-pressure applications, such as marine engines that run at constant speeds. Steady state maps are not sufficient to accurately predict performance. Researchers, and at least one manufacturer [2–4], have investigated integrating unsteady effects into turbine maps. Some of the findings showed that pulsating effects can lead to performance prediction deviations from -18% to 12% for a range of turbine speeds [2]. The creation of steady state maps also typically relies on a narrow range of test data supplemented by data extrapolation techniques. These extrapolation methods can lead to performance prediction deviations of up to 10% at low blade speed ratios [5].

This raises a problem; how can we predict the effect of pulsating flow phenomena on performance? It's possible to use CFD to achieve a reasonably accurate picture of pulsating flow effects, but this is time consuming and computationally expensive. Cao and Xu [6] proposed an unsteady quasi-3D model which reduced computational time, and Chen [7] proposed a similar model using only the Euler equations. This code aims to build from a previously unpublished code produced by Chen.

NOMENCLATURE

Roman

A	Amplitude/Area (m^2)
b	Flow passage width (m)
C_f	Coefficient of friction
C_p	Specific heat at constant pressure (J/kg)
dt	Time step (s)
dx_r	Length of rotor segments (m)
h	Specific enthalpy (J/kg)
I	Index value for position identification
J	Index value for position identification
L	Wet periphery of the flow passage (m)
LE	Rotor leading edge
P	Pressure (Pa)
Q	Heat transfer (J/kg-s)
R_r	Radius of the rotor flow passage (m)
St	Strouhal Number
t	Time (s)
T	Temperature (K)
V	Absolute velocity (m/s)
W	Relative velocity (m/s)
x	Location coordinate along the flow axis (m)

Greek

α	Angle between absolute and peripheral velocity
η	Cycle mean total-to-static efficiency
λ	Characteristic line
ρ	Density (kg/m3)
τ	Time scale
Φ	Phase difference between pressure and temperature waves/Azimuth angle
ω	Angular frequency (rad/s)
Ω	Rotor angular speed (rad/s)
ψ	Mass withdrawal/addition per unit length, per unit volume (kg/s-m)

Subscripts

0	Stagnation/total, turbine casing inlet
1	Centroid of turbine casing
3	Position in casing immediately before rotor inlet
4	Position in immediately inside rotor leading edge
5	Position in rotor immediately inside rotor exit
6	Position immediately outside rotor exit
atm	Atmospheric
c	Casing
F	Fluid
is	Isentropic
m	Mean
P/p	Pressure/Pulse
r	Rotor
T	Temperature
w	Wall of casing housing

BACKGROUND

Predicting the performance of a turbocharger subject to pulsating flow is complex. When predicting steady-state performance there are two independent non-dimensional parameters (expansion ratio and tip Mach number) that determine mean cyclic performance metrics. When looking at unsteady performance, if you assume that a pulsating inlet flow occurs as a simple sinusoidal wave, there are four additional non-dimensional parameters that also affect mean turbine performance. These new parameters are in addition to the two that already existed in steady-state conditions. With the aforementioned sinusoidal wave assumption, the incoming pressure and temperature waves can be represented by equations 1 and 2.

$$P(t) = A_P \sin(\omega t) + P_{0m} \quad \text{EQ1}$$

$$T_0(t) = A_T \sin(\omega t + \Phi) + T_{0m} \quad \text{EQ2}$$

Where Φ is the phase difference between the pressure and temperature waves. The four new non-dimensional variables here are the non-dimensional total amplitude of pressure (A_P/P_{0m}) and the non-dimensional total amplitude of temperature (A_T/T_{0m}), along with the phase difference (Φ) and the Strouhal number (ω/Ω), where Ω is the angular speed of the rotor. All of these affect cyclic mean performance.

Strouhal number may be used as an expression of the relative importance of unsteadiness in oscillating gas flows [8], and can be represented by the ratio of the time taken for a fluid particle to pass through the turbine components (τ_F), and the time scale of the unsteadiness in the pulsating gas flow (τ_p) [9]:

$$St_{F-P} = \frac{\tau_F}{\tau_P} \quad \text{EQ3}$$

As a rough guide, if this Strouhal number is close to one, both quasi-steady and unsteady effects are important, and should be accounted for in any model. Values much larger than one represent the domination of unsteady effects, and values lower than one suggest that quasi-steady effects are dominant.

Some pulsating flow models represent the rotor differently to the volute section (i.e. with an unsteady volute model, and quasi-steady rotor model), in this case a second Strouhal number may be important [9]:

$$St_{r-p} = \frac{\tau_r}{\tau_p} \quad \text{EQ4}$$

where the time scale for the rotor to spin for one complete revolution (τ_r) is independent of τ_F. When the value of Str_{r-p} is small, steady effects may govern performance. This model was built from scratch with the entire flow path treated as unsteady, therefore the flow in both the volute and the rotor is treated in an unsteady manner.

Initial zero-dimensional modelling attempts at addressing pulsating flows in turbines were made by Dale and Watson [10,11] and continued by others[12–14]. This methodology was later superseded by models based upon one-dimensional gas-dynamics equations. The majority of zero-dimensional and one-dimensional nozzle models are unable to simulate the circumferential feeding of the rotor from the turbine casing.

Researchers have also ventured into 3D modelling of pulsating flow in a turbocharger by adopting the Navier-Stokes equations. This involves adopting two frames of reference, with one representing the stationary zones (volute) and another for the rotating (rotor) regions. The "frozen rotor" method involves ignoring the relative motion of each of these sub-domains, such as the study by Lam et al. [15] Another attempt by Palfreyman and Martinez-Botas was conducted whilst explicitly rotating the rotor during the calculation. [16]

MODEL DESCRIPTION

The model presented here allows circumferential feeding of the rotor, similar to previous work by Chen [7,17], however this new code uses an unsteady rotor model and has many other differing assumptions and equations. This new code has been modernized into the C++ programming language to enable simpler expansion in the future, and integration with other one-dimensional gas dynamics codes.

This one-dimensional model predicts the performance of a vaneless radial turbine under pulsating inlet conditions, using the 1D Euler equations for turbomachinery. Figure 1 represents the stations used within the model. Free vortex flow is allowed between the volute centroid and exit (1-3), and a vaneless space loss model is applied before rotor entry. Circumferential feeding of the rotor from the casing is simulated, with the number of equidistant data points along the casing flow axis equal to the number of rotor blades (See Figure 5).

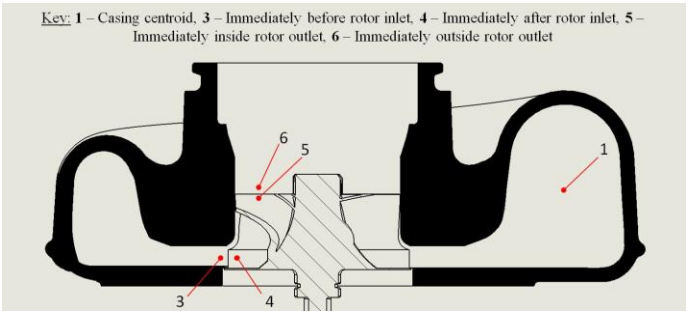

Figure 1- Diagram showing the numbering convention used in modelling.

During unsteady operation, gas flow enters the volute of a turbocharger and exits via the rotor, but unlike steady-flow, the flow is a function of time at each operating point, and may reverse (with flow exiting the rotor, back into the volute). In this model the volute is treated as unsteady, with a term to account for mass addition and withdrawal (Ψ). The one-dimensional form of the Euler equations [18,19] are adapted as follows for the volute; continuity equation for the volute:

$$\frac{\partial P_1}{\partial t} + \frac{\partial \rho_1 V_1}{\partial x_1} = \frac{\Psi}{A_1} - \frac{\rho_1 V_1}{A_1}\frac{dA_1}{dx_1} \quad \text{EQ5}$$

where Ψ is mass addition and withdrawal to and from the volute. This term is part of the continuity, momentum and

energy equations (except for points within the casing inlet section) and is calculated as:

$$\Psi = -\rho_3 V_3 \, sin(\alpha_3) b_3 R_3 \, / \, R_1 \qquad EQ6$$

Momentum equation for the volute:

$$\frac{\partial \rho_1 V_1}{\partial t} + \frac{\partial \rho_1 {V_1}^2}{\partial x_1} = \frac{\Psi}{A_1} V_3 \cos(\alpha_1 - \alpha_3) - \frac{\rho_1 {V_1}^2}{A_1}\frac{dA_1}{dx_1} - \frac{L_1}{A_1} sign(V_1)\tau_w \qquad EQ7$$

Where τ_w is the wall shear stress:

$$\tau_w = C_{f0/fc} \rho_1 {V_1}^2 \qquad EQ8$$

Energy equation for the volute:

$$\frac{\partial \rho_1 h_{01} - P_1}{\partial t} + \frac{\partial P_1 V_1 h_{01}}{\partial x_1} = \frac{\Psi}{A_1} h_{03} - \frac{\rho_1 V_1 h_{01}}{A_1}\frac{dA_1}{dx_1} + \rho_1 Q \qquad EQ9$$

where Q is the heat transfer through the wall of the turbine casing:

$$Q = C_{f0/fc} \frac{L_1}{A_1} V_1 \left(T_w - T_1 - \frac{0.424 {V_1}^2}{C_p} \right) \qquad EQ10$$

The first order Lax-Friedrichs finite difference method is then used for solution of the equations 5, 7 and 9 to find values of density, pressure and velocity for each new time step; further details of the calculation process for the casing section can be found in Figure 4. At the tongue of the casing, the end is assumed to be closed and therefore velocity is set to zero, and the method of characteristics is used to calculate pressure and density. When inflow from the volute to the rotor occurs (regular operation), the method of characteristics is used to solve along with the λ_- compatibility equation, and an incidence loss model is then applied upon entry to the turbine rotor. If reversed flow occurs, and there is an inflow from the rotor to the turbine casing, the incidence loss model is replaced with the solution to the λ_0 compatibility equation at the rotor inlet boundary.

For the rotor, the Lax-Friedrichs method is also used to solve for internal points of the rotor flow passages. Equations are based upon those presented in previous studies [20–22] and a basic loss model is used. A set of rotor equations, as they are used in the code, can be found in the appendix of this paper.

MODELLING INFORMATION FLOW

To illustrate how the model operates, a number of flow charts have been created to demonstrate the information flow throughout the code. The code is formed of 6 main sections; these are listed below along with a brief description of their purpose and argument inputs and outputs. It is worth noting, that as well as the listed arguments each subroutine can update the values of global variables.

- MAIN(…) - This section is the main section of the code, primarily responsible for controlling the flow of information and containing calls to other subroutines.
- EXIT(…) – Subroutine for solving boundary equations for reversing flow at the rotor exit. Argument in: relative velocity at rotor exit, argument out: relative error of velocity.
- CHAR(…) - Subroutine for solving boundary equations using the method of characteristics to find the speed of sound, flow velocity, density and pressure at a given characteristic. Arguments in: index of boundary point, characteristic description (left or right running, λ_0, λ_- or λ_+ Mach lines), mass addition (on or off). Arguments out: speed of sound, flow velocity, density and pressure at the given characteristic.
- ENTRY(…) - Subroutine to solve boundary equations for the entry of the rotor. Argument in: absolute flow angle immediately before rotor leading edge, relative error of pressure.
- CASING(…) - Subroutine interpolates parameters at position 3 in the casing axis. Argument in: parameter to be interpolated, argument out: interpolated value.
- THROAT(…) - Subroutine interpolates parameters at position 3 in the casing throat. Argument in: parameter to be interpolated, argument out: interpolated value.

Figure 2 shows two loops used to determine dt for the casing (thick dashed lines) and rotor (fine dashed lines); the smaller of these two values becomes the time step for the iteration. Equations used here can be found in the appendix. Before calculating the time step, the code reads input data and uses these inputs to form various parameters, constants and coefficients used throughout the calculation, as well as forming initial values for time varying parameters such as the pulsating inlet pressure and temperature waves, and the density, pressure and velocity at different points throughout the casing.

Figure 3 illustrates the casing analysis section, which follows on immediately after time step determination shown in Figure 2. After calculating shear stress and heat transfer values, the right hand side of the Euler equations (Equations 5, 7 and 9) are calculated for each internal point of the volute. In each case the mass addition/withdrawal terms are included, unless the point in question is part of the inlet to the casing.

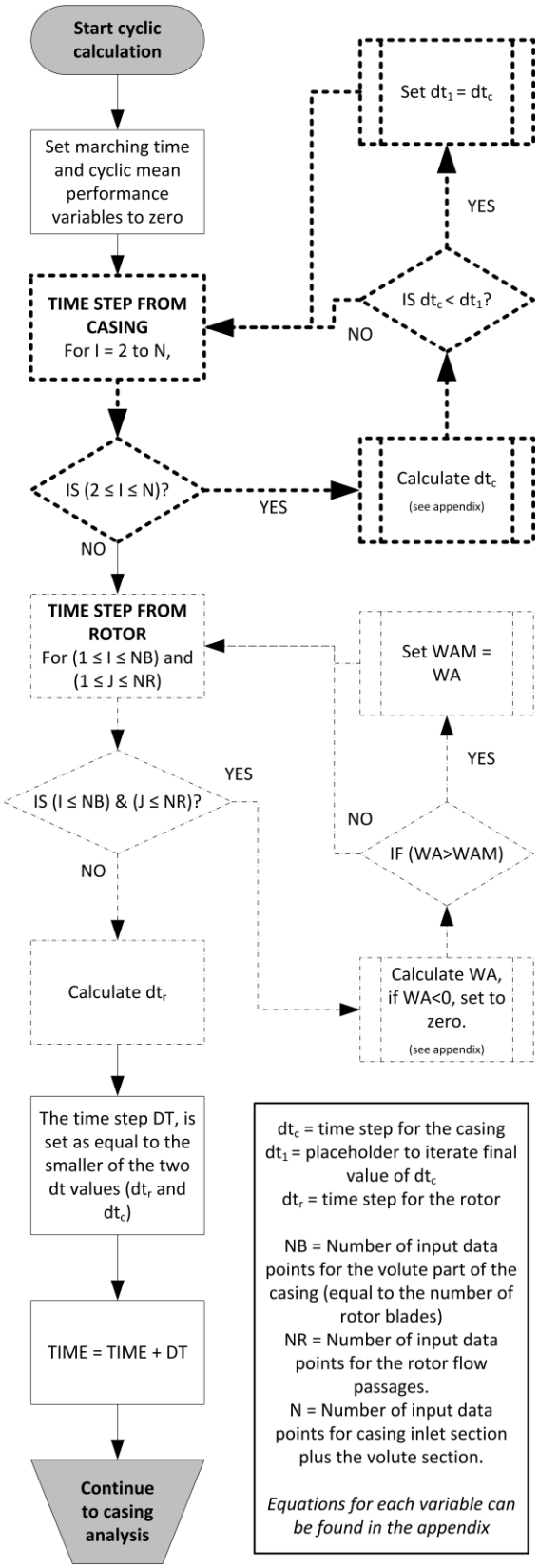

Figure 2- Flowchart showing time step selection process. WAM is initially set to zero. (See appendix 2 for time step equations)

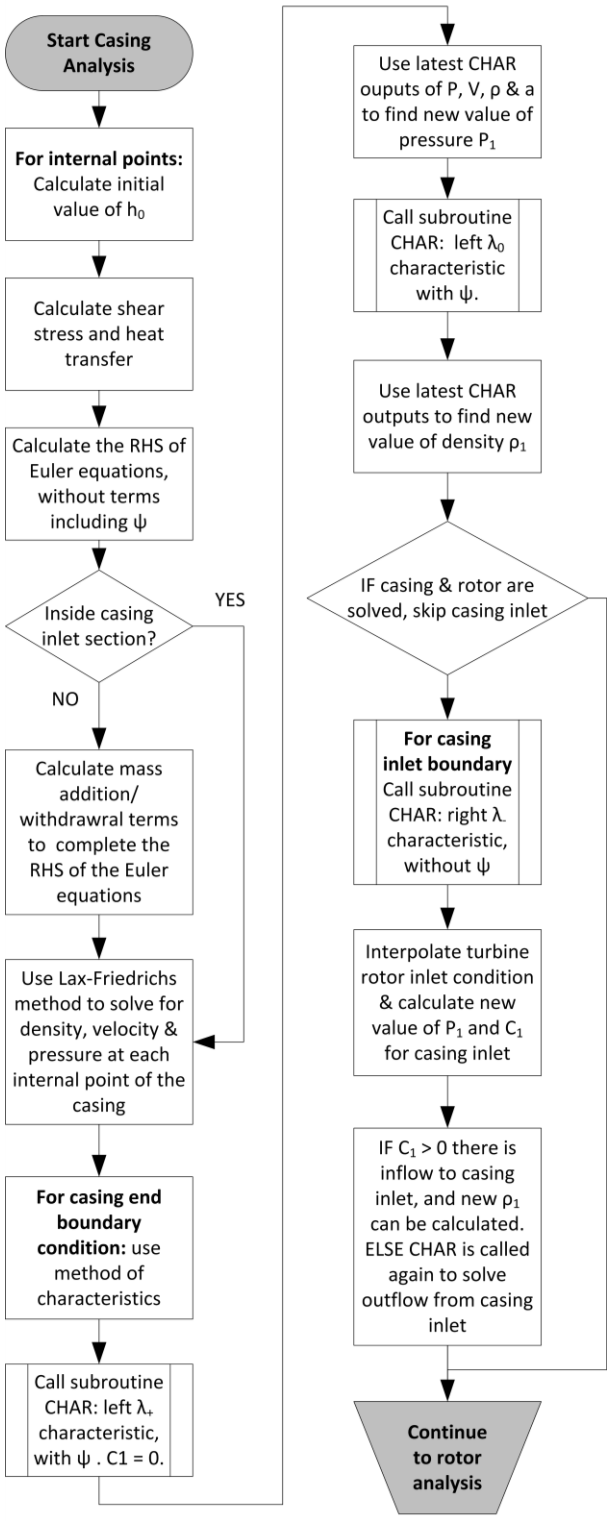

Figure 3- Flowchart showing the process of casing analysis

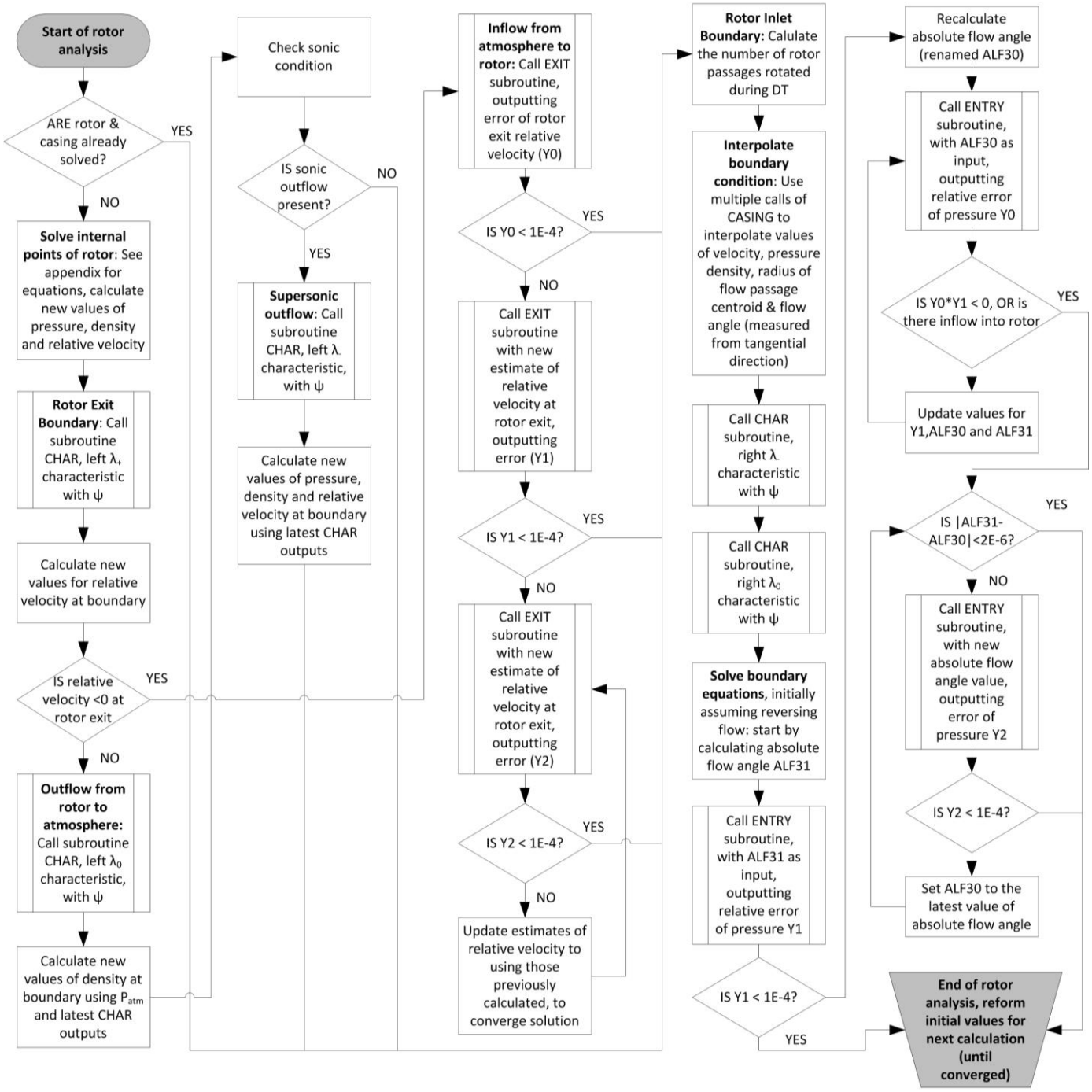

Figure 4- Flowchart showing the information flow during analysis of the rotor

Figure 4 shows the information flow through the rotor analysis procedure. After checking a previous iteration hadn't solved the entire rotor and casing, the code solves for each internal point of the rotor, and for every flow passage. If we have an outflow from the rotor to the atmosphere, the method of characteristics is adopted at the boundary and the sonic condition is checked; if necessary the method of characteristics is used again before moving on to the rotor inlet boundary. After interpolating conditions required to use the method of characteristics at the rotor inlet boundary, remaining variables are formed before calculating the solution of the remaining equations. Once the rotor analysis is complete, the code moves outside of the cyclic loop to reform variables and check convergence before restarting the casing and rotor loops if necessary.

INPUT DATA

A pulsating input condition was used in order to calculate the performance of the turbine subject to unsteady flow. The pulse is characterized by equation 11:

$$P_0(t) = 1.42e^5 - 2.02e^4 \sin\left(\frac{t\pi}{180}\right) \qquad EQ11$$

A plot of this sinusoidal pulse can be seen in Figure A1 (appendix 3) and is used here as a general case, however if the pulse profile of the engine exhaust is known through experiment or otherwise, an expression to describe its profile may be substituted for EQ11. In addition to pressure, the time-varying inlet temperature wave was defined by equation 12. The calculation runs for one pulse period, which in this case was defined as 1/70 seconds, and both the inlet pressure and temperature waves were defined with 360 data points according to equations 11 and 12.

$$T_0(t) = T_{0,m}\,\frac{P_0(t)^{\frac{\gamma-1}{\gamma}}}{P_{0,m}} \qquad EQ12$$

Table 1- Selected inputs to the code for pulsating flow prediction

Number of casing inlet data points	5
Number of data points for casing	12
Number of rotor blades	12
Number of rotor passage data points	5
Rotor inlet radius	0.0485 m
Rotor outlet RMS radius	0.3242 m
Rotor exit blade angle	0.8831 rad
Rotor inlet blade height	0.0171 m
Rotor exit blade height	0.0273 m
Shroud clearance at leading edge	2.452E-4 m
Shroud clearance at trailing edge	2.452E-4 m
Inlet pulse frequency	70 Hz
Inlet average temperature	400 K
Wall temperature	320 K
Ambient pressure	1.0133E5 Pa
Ambient temperature	300 K

Table 1 shows some of the key inputs to the code, the number of points that are calculated is determined by user input. As well as the input data shown in Table 1, a number of matrix inputs are required These include the area of the casing flow passage, radius of the casing flow passage centroid and length of the casing segments, area of the rotor flow passages, radius of the rotor flow passage centroid and wet periphery of the casing and rotor flow passage centroids, amongst others.

Since the model uses a sliding rotor interface, these matrix inputs should match up to the number of inlet data points (e.g. if the casing is split into 12 sections, the area and radius of the casing flow passage must be provided for 12 equally spaced locations). In this case, the area of the casing converged from a maximum of $4.462e^{-3}$ m^2 to $2.39e^{-4}$ m^2, with radius values ranging from $8.0779e^{-2}$ m to $4.9922e^{-2}$ m. Geometric data for the rotor passages is input similarly.

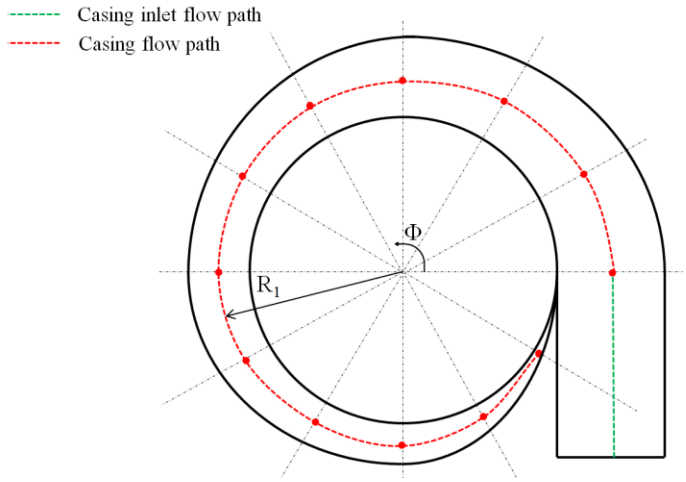

Figure 5- Diagram showing division of the casing volute into 12 equally spaced data points, equal to the number of rotor flow passages.

PULSATING FLOW RESULTS

Figures 6 – 9 show the resulting plots of running the unsteady flow model with a frequency of 70 Hz. Encouragingly, hysteresis can be observed in both the non-dimensional mass flow locus (Figure 6) and the plot of total-to-static efficiency and blade speed ratio (Figure 7), matching the findings of past studies on pulsating inlet flows to radial turbines. [9,10]

Drawn to the same scale on the y-axis, Figures 8 and 9 show the variation of absolute flow angle of gas entering the rotor immediately before the leading edge at two different azimuth locations in the turbine housing. The blue lines show raw data taken from the output of the code, and the solid black lines show the average value measured across one pulse period.

Figure 8 illustrates a more erratic fluctuation in the flow angle close to the tongue of the volute (azimuth angle = 330 degrees) when compared to other points in the volute, such as the position of 180 degrees azimuth angle illustrated in Figure 9. This finding is in agreement with the previous model by Chen [9], which also had the capability to simulate circumferential filling of the rotor from the casing.

Figure 7 compares the effects of pulse shape on the unsteady efficiency locus. The two pulse profiles used to produce this chart are plotted in appendix 3; both pulse profiles have the same maximum, minimum and average values. The key difference is the greater area enclosed between the sinusoidal waveform and the average value. This leads to a drop in cycle averaged efficiency from 69.44% to 68.79%.

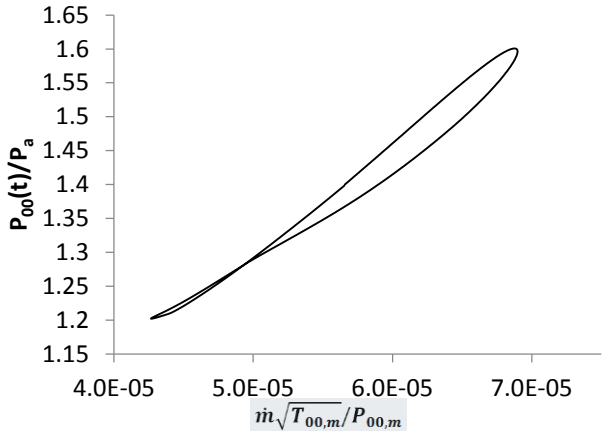

Figure 6- Mass flow locus at 70 Hz

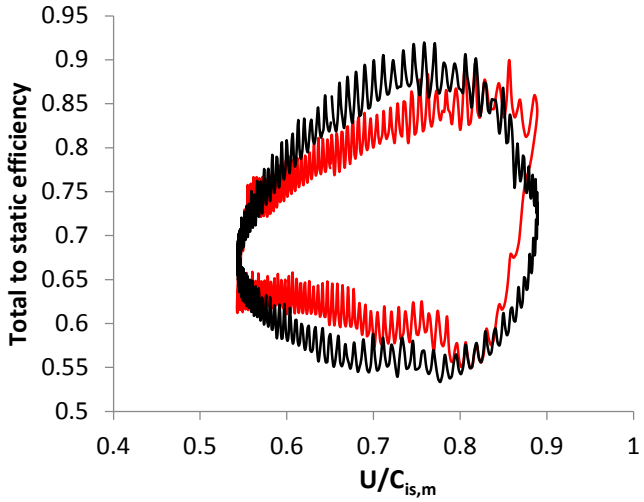

Figure 7- Efficiency locus for linear (red) vs. sinusoidal (black) pulse profiles. See appendix 3 for plots of the pulse profiles.

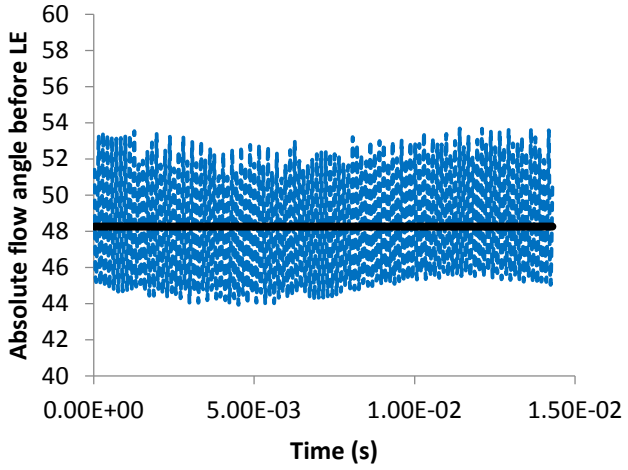

Figure 8- Flow angle variation, at a 330 degrees azimuth angle

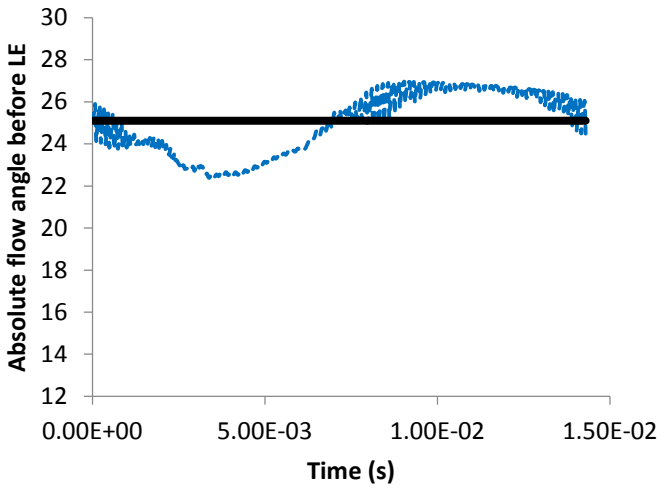

Figure 9- Flow angle variation, at a 180 degrees azimuth angle

SUMMARY

A one-dimensional model of a vaneless radial inflow turbine has been created, which allows for circumferential feeding of the rotor from the turbine casing. After a simulation of a turbine subject to pulsating inlet conditions of a given frequency, results were found to replicate the hysteresis effects within the mass flow and efficiency loci that have been observed in past studies on pulsating flow. Given the simplifications present in the current model this agreement with previous findings, as discussed in 'Pulsating Flow Results' is encouraging. Further agreement with previous findings is observed as the fluctuation of flow angle at the rotor leading edge is most prevalent close to the tongue of the volute, and dampened in the rest of the housing.

Extensions to this model are currently being developed, and the following improvements are currently being worked upon:

- A new boundary condition at the tongue, to allow for flow to rejoin the main flow after one revolution of the volute.
- Improved heat transfer model based upon on-engine experimentation, which has been designed to gather pulsating flow and heat transfer data.
- Variable geometry loss model, enabling the current vaneless space to be replaced with a variable geometry stator when required. Station 2 will be introduced to represent the inlet to the stator.
- The current Lax-Friedrichs solver can be improved by adopting the second-order Lax-Wendroff method
- Modifications to the meanline flow path may allow the model to simulate mixed-flow turbines, and be validated against relevant unsteady data

Appendix 1 – Rotor Equations

In the following equations, I and J are the index values that point to values for the particular rotor location currently being calculated. For the examples included in this study, there are 12 rotor blades (I = 12) and each of the resulting rotor flow passages contain 5 points for calculation along the flow mean-line (J = 5). Matrices for density (ρ_r), relative velocity (W_r) and pressure (P_r) contain the respective values for each point required for calculation, acquired during the previous iteration. The following equations are used to find new values of density, relative velocity and pressure for the internal points of the rotor. ***Note: an under-bar is used here to denote newly calculated values, and does not refer to any mathematical operator.***

$$\underline{\rho_r}[I,J] = \frac{\rho_r[I,J+1] + \rho_r[I,J-1]}{2} - DTXR(Z1_r - Z2_r) + F_1 DT$$

$$\underline{W_r}[I,J] = \frac{1}{\underline{\rho_r}[I,J]}\left[\frac{Z1_r + Z2_r}{2} - DTXR(Z1_r W_r[I,J+1] + P_r[I,J+1] - Z2_r W_r[I,J-1] - W_r[I,J-1]) + F_2 DT\right]$$

$$\underline{P_r}[I,J] = \left[\frac{1}{2}\left(\rho_r[I,J+1]h_{01,r} - P_r[I,J+1] + \rho_r[I,J+1]h_{02,r} - P_r[I,J+1]\right) - DTXR\left(Z1_r h_{01,r} - Z2_r h_{02,r}\right) + (F_3 DT) - \underline{\rho_r}[I,J]\,\underline{W_r}[I,J]\frac{W_r[I,J]}{2}\right](\gamma - 1)$$

Where:

$$Z1_r = \rho_r[I,J+1]W_r[I,J+1]$$

$$Z2_r = \rho_r[I,J-1]W_r[I,J-1]$$

$$h_{01,r} = \frac{\gamma}{\gamma - 1}\left(\frac{P_r[I,J+1]}{\rho_r[I,J+1]}\right) + W_r[I,J+1]\left(\frac{W_r[I,J+1]}{2}\right)$$

$$h_{02,r} = \frac{\gamma}{\gamma - 1}\left(\frac{P_r[I,J-1]}{\rho_r[I,J-1]}\right) + W_r[I,J-1]\left(\frac{W_r[I,J-1]}{2}\right)$$

DTXR is half of the time step (DT) divided by the length of the rotor segments dx_r. The coefficients F_1, F_2 and F_3 were calculated prior to the above calculations, as per the following equations:

$$F_1 = -\rho_r[I,J]\,W_r[I,J]\left(\frac{A_r[J+1] - A_r[J-1]}{\frac{dx_r}{2}}{A_r[J]}\right)$$

$$F_2 = \rho_r[I,J]\Omega^2 R_r[I]\left(\frac{R_r[J+1] - R_r[J-1]}{\frac{dx_r}{2}}\right) + F_1 W_r[I,J] - F_r\rho_r[I,J]\,W_r[I,J]^2 L_r sign(1, W_r[I,J])$$

$$F_3 = F_1\left(\frac{\gamma}{\gamma - 1}\frac{P_r[I,J]}{\rho_r[I,J]} + W_r[I][J]\frac{W_r[I,J]}{2}\right) + Q\,\rho_r[I,J]$$

Where Q is expressed as:

$$Q = F_r W_r[I,1]L_r[J]C_p\left(T_w - \frac{\frac{P_r[I,J]}{\rho_r[I,J]}}{R} + \frac{0.424}{C_p}W_r[I,J]^2\right)$$

R_r is the radius of the rotor flow passage. F_r is the friction coefficient of the rotor flow passage and L_r is the wet periphery of the rotor flow passage. dx_r is the length of the rotor segments.

Appendix 2 – Equations for the calculation of time step variables:

Time step for the casing dt_c is found by iterating the following equations across every casing data point (inlet and volute sections). In this case the index $[I]$ denotes the position in the casing inlet or volute.

$$dt_c = \frac{dx_c[I-1]}{CA}$$

$$CA = |C_1[I]| + \sqrt{\frac{\gamma P_1[I]}{\rho_1[I]}}$$

The rotor time step dt_r is calculated by iterating the equation for WA, to find WAM as described in the flow chart, then inserting that value into the equation for dt_r:

$$dt_r = \frac{dx_r[I-1]}{WAM}$$

$$WA = |W_R[I,J]| + \sqrt{\frac{\gamma P_R[I,J]}{\rho_R[I,J]}}$$

For the case of the rotor equations for WA and dt_r, the indices $[I, J]$ denote the flow passage under consideration, and the position within that flow passage. For example, I = 12 denotes the 12th flow passage in the rotor, and J = 2 denotes the second point for calculation within that flow passage.

Appendix 3 – Pressure pulse plots

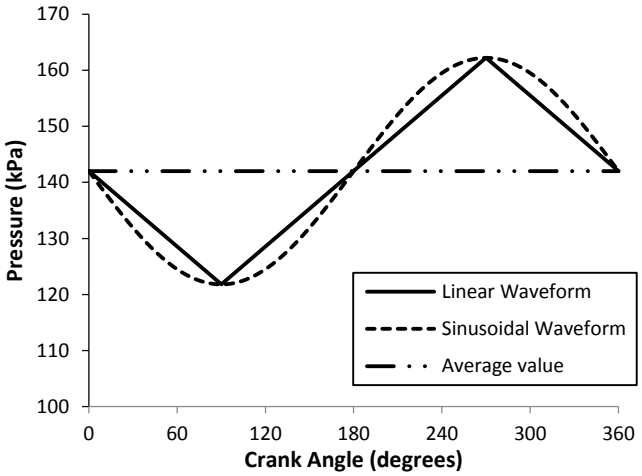

Figure A1- Linear pressure pulse used to generate comparison in Fig. 10 plotted with the sinusoidal pulse described by equation 11. Both pulses have the same minimum, average and maximum values.

REFERENCES

[1] Markets, R. and, 2015, "Turbocharger Market by Vehicle Type (On-Highway (Passenger Car, LCV, & HCV), Off-Highway (Agricultural Tractors & Construction Vehicles)), Locomotive, Technology (VGT/VMT & Wastegate), Fuel Type (Gasoline & Diesel), & by Region - Forecast to 2020", Dublin, Ireland. Available Online: <http://www.marketsandmarkets.com/Market-Reports/turbochargers-market-919.html>. Accessed 23/07/2016.

[2] Pesiridis, A., Lioutas, S., and Martinez-Botas, R. F., 2012, "Integration of Unsteady Effects in the Turbocharger Design Process," Proceedings of ASME Turbo Expo 2012, GT2012-69053.

[3] Chiong, M. S., Rajoo, S., Costall, A., Bin Wan Salim, W. S.-I., Romagnoli, A., and Martinez-Botas, R. F., 2013, "Assessment of Cycle Averaged Turbocharger Maps Through One Dimensional and Mean-Line Coupled Codes," Proc. ASME Turbo Expo 2013, GT2013-95906.

[4] Gugau, M., and Roclawski, H., 2012, "On The Design and Matching of Turbocharger Turbines for Pass Car Gasoline Engines," Proceedings of ASME Turbo Expo 2012, GT2012-68575.

[5] Pesiridis, A., Salim, W. .-I. W., and Martinez-Botas, R. F., 2012, "Turbocharger matching methodology for improved exhaust energy recovery," 10th IMechE International Conference on Turbochargers and Turbocharging, Elsevier, pp. 203–218. DOI: 10.1533/9780857096135.4a.203

[6] Cao, T., and Xu, L., 2014, "A Low Order Model for Predicting Turbocharger Turbine Unsteady Performance," ASME Turbo Expo 2014, GT2014-25913. DOI:10.1115/GT2014-25913

[7] Chen, H., 1990, "Steady and Unsteady Performance of Vaneless Casing Radial-Inflow Turbines," Ph.D. Thesis, University of Manchester.

[8] Greitzer, E., 1985, "An Introduction to Unsteady Flow in Turbomachines," Thermodyn. Fluid Mech. Turbomach., II of NATO (Series E: Applied Sciences), pp. 967–1025.

[9] Chen, H., and Winterbone, D. E., 2014, "A one-dimensional performance model for turbocharger turbine under pulsating inlet condition," 11th IMechE International Conference on Turbochargers and Turbocharging, pp. 113–123. DOI: 10.1533/978081000342.113

[10] Dale, A., and Watson, N., 1986, "Vaneless Radial Turbocharger Turbine Performance," Proceedings of the Institution of Mechanical Engineers, 3rd IMechE International Conference on Turbocharging and Turbochargers, IMechE, London, UK.

[11] Dale, A., 1990, "Vaneless Radial Turbocharger Turbine Performance," Ph.D. Thesis, Imperial College, University of London.

[12] Yeo, J., 1990, "Pulsating Flow Behaviour in a Twin-Entry Vaneless Radial-Inflow Turbine," IMechE Turbocharging Conference, IMechE, London, UK, pp. 113–122.

[13] Baines, N., and Yeo, J., 1991, "Flow in a Radial Turbine under Equal and Partial Admission Conditions," IMechE C423/002, IMechE, London, UK.

[14] Baines, N. C., Hajilouy-Benisi, A., and Yeo, J. H., 1994, "The pulse flow performance and modelling of radial-inflow turbines," Proceedings of IMechE International Conference on Turbochargers and turbocharging, IMechE, London, UK, pp. 209–218.

[15] Lam, J. K.-W., Roberts, Q. D. ., and McDonnell, G. ., 2002, "Flow Modelling of a Turbocharger Turbine under Pulsating Flow," Proceedings of IMechE, Part C: Mech. Eng. Sci. C602/025/2002, IMechE, London, UK.

[16] Palfreyman, D., and Martinez-Botas, R. F., 2005, "The Pulsating Flow Field in a Mixed Flow Turbocharger Turbine: An Experimental and Computational Study," J. Turbomach., 127(1), p. 144.

[17] Chen, H., Hakeem, I., and Martinez-Botas, R. F., 1996, "Modelling of a turbocharger turbine under pulsating inlet conditions," Proc. Inst. Mech. Eng. Part A J. Power Energy, 210(5), pp. 397–408.

[18] Zucrow, M., and Hoffman, J., 1977, "Gas Dynamics, Volume 2: Multi-Dimensional Flow", John Wiley and Sons, Inc.
[19] Woods, W. ., and Allison, A., 1976, “Unsteady compressible flow with gradual mass addition and area change,” Proceedings of IMechE Sixth Thermodynamics and Fluid Mechanics Convention, IMechE, London, UK, pp. 179–186.
[20] Mizumachi, N., Yoshiki, D., and Endoh, T. A., 1979, “A Study on Performance of Radial Turbine Under Unsteady Flow Conditions,” Rep. Inst. Indust. Sci., Univ. Tokyo, 28(1), pp. 1–77.
[21] Wasserbauer, C. A., and Glassman, A. J., 1975, “FORTRAN program for predicting off-design performance of radial-inflow turbines,” NASA Tech. Pap., (TN D-8063), p. 55.
[22] Todd, C., and Futral, S., 1969, “Fortran IV program to estimate the off-design performance of radial-inflow turbines.”, NASA Technical Note TN D-5059.